doi.org/10.1002/batt.201900227

Fabrication of Current Collectors and Binder-Free Electrodes on Separators Used in Lithium-Ion Batteries

Nicolas Delaporte,[a] Diby B. Ossonon,[a] Karim Zaghib,*[b] and Daniel Bélanger*[a]

We report the fabrication of a composite electrode through the deposition of electrode materials directly onto a separator to avoid the use of a metallic current collector. In addition to being an active electrode material, this method employs only graphene as both a carbon additive and a binder. A major achievement is the elimination of heavy and inactive current collector, harmful solvents, and resistive binder. The deposition of the composite film electrode was applied through the filtrated dispersion of a redox active material and graphene through a separator (Celgard), which is commonly used in battery. The electronic conductivity of $LiFePO_4$/Celgard electrodes was ~10 times higher than that of conventional electrodes spread onto an aluminum current collector. The electrochemical performances of $LiFePO_4$/C (LFP) and $Li_4Ti_5O_{12}$ (LTO) half-cells fabricated according to this process and a conventional method were compared. A clear improvement in the electrochemical performance for electrodes fabricated using the new method was observed, particularly at high C-rates. $LiFePO_4$/Celgard electrodes deliver specific capacities of up to 125 $mAh.g^{-1}_{electrode}$ corresponding to more than 6 times the gravimetric capacity of an LFP electrode coated on Al foil. A $LiFePO_4/Li_4Ti_5O_{12}$ full cell made using film electrodes deposited on a Celgard membrane shows stable specific capacities during the cycling at various C-rates and delivers a specific capacity of 106 $mAh.g^{-1}_{electrode}$ at a C/10 rate.

1. Introduction

Electrochemical energy storage with lithium-ion batteries is extremely attractive and has become widespread for various applications including the development of electric vehicles. This is leading researchers and industries to reduce battery pack costs and increase their energy density by manufacturing batteries using novel electrode processing and engineering techniques.[1,2] A lithium-ion electrode fabrication technique depends on the cell chemistry, amount of materials available, applications, and production requirements. Most commercial lithium-ion cells are produced in extremely large quantities and require low-cost and scalable fabrication methods.[3] Such fabrication methods must be adapted to targeted applications such as those for microelectromechanical systems,[4] biomedical sensors,[5] or wireless sensors,[6] which require electrochemical cells of a few micrometers or millimeters in diameter. Three-dimensional printing remains the best method for a micro-battery design,[7,8] and although reserved for small electrochemical devices, this technology can potentially double the energy density by optimizing the limited space available.[9] Thin film electrodes of a few nanometers formed on a substrate are obtained through spin coating although the process is difficult to scale.[10,11] Among other electrode fabrication techniques, a paste generating method generally applies an active electrode material,[12] a conductive carbon additive[13] (e.g., carbon nanotubes[14] or Ketjen black),[15] and a thickener fluoropolymer such as polytetrafluoroethylene (PTFE).[16] The paste is then deposited onto a current collector (e.g., a stainless steel mesh) and pressed. This method leads to thick electrodes but with small dimensions. A freeze-casting process is an unconventional method for preparing electrodes with a highly interconnected microscale pore structure.[17] A typical procedure consists of rapidly freezing a solution containing electrode materials, and the frozen solvent is subsequently removed through freeze-drying, forming a macroporous structure.[18] However, this method is time-consuming, unscalable, and costly. Electrospinning permits the fabrication of active material fibers, and a self-standing film can be obtained without the addition of a binder.[19] This fabrication process is too time consuming to be implemented in industry and yields a small number of electrodes. Other fabrication methods such as solvent-based electrostatic spray deposition,[20–22] pulsed laser and sputtering deposition,[23,24] and dry painting[25] suffer from slow deposition rates and high annealing temperature.[26] Screen printing[27] consisting of reproducing a desired template with a diluted suspension of a carbon, binder, and electroactive material is limited to electrodes of small dimensions, but leads to extremely thin films (few micrometers). The quality of an electrode is strongly dependent on the quality of the ink (i.e., the viscosity and surface tension).[28,29] Extrusion methods are also employed to reduce the amount of solvent,[30] or when several polymers are used in the composition of an electrode and are insoluble in any solvent. A solvent-free roll-to-roll manufacturing technique was recently introduced, and consists

[a] Dr. N. Delaporte, Dr. D. B. Ossonon, Prof. D. Bélanger
Département de Chimie, Université du Québec à Montréal
Case Postale 8888, Succursale Centre-Ville
Montréal, Québec, H3 C 3P8, Canada
E-mail: belanger.daniel@uqam.ca
[b] Dr. K. Zaghib
Hydro-Québec
Center of Excellence in Transportation Electrification and Energy Storage
Varennes, Québec, J0 L 1 N0, Canada
E-mail: zaghib.karim@hydro.qc.ca

Supporting information for this article is available on the WWW under https://doi.org/10.1002/batt.201900227

of forming a self-standing film by pressing the active material and carbons between rolls at a pressure of above 20 MPa.[31,32]

Large-scale manufacturing of lithium-ion batteries is dominated by the so-called web-coating method, the industrial version of a doctor-blade generally employed in laboratories to spread slurry on a current collector foil.[33] A web-coating is the best method among all of the above electrode fabrication techniques because an electrode prepared on a solid current collector is easy to handle, and because the method is efficient, cost effective, and yields a large number of electrodes.[3] However, some technical and environmental issues remain to be addressed with this fabrication method. In most cases, electrodes are fabricated using a polyvinylidene fluoride (PVDF) binder dissolved in a solvent, typically, N-methyl-2-pyrrolidone (NMP).[34] NMP is a volatile organic compound and owing to its high toxicity and flammability needs to be captured using a chemical process such as condensation or vacuum distillation, which significantly increases the overall cost of the electrode coating.[35] Moreover, drying such electrodes consumes significant amounts of energy owing to a high boiling point (204.3 °C) and low vapor pressure of NMP (1 mm Hg at 40 °C).[36] PVDF and other fluoropolymer-based binders are widely employed because of their electrochemical stability and strong adhesion to a metal foil owing to metal-O, metal-F, or metal-C bonds following the drying procedures.[37] This denaturation of the binder leads to an increase in the cell impedance and a loss of electrode integrity. Finally, the binder is generally costly and electroinactive, and for these reasons, its quantity does not generally exceed 5 wt% in the electrode composition.[38] For instance, although greener processes employing sodium carboxymethyl cellulose (CMC) as a low-cost binder and water as a solvent have been developed,[39–41] some major issues have yet to be solved. First, aqueous slurries suffer from poor wettability onto the current collectors,[42] which are also prone to corrosion, particularly aluminum foil.[43] In addition, water-based electrodes present an agglomeration effect, poor ink homogeneity, and residual moisture after drying, which dramatically shorten the cycle-life of the batteries.[44] Traces of water in common organic liquid electrolytes can lead to metal dissolution and the formation of a passivation layer.[45] Moreover, the ageing of active materials upon exposure to water is also a problem that remains to be considered prior to a scale-up.[46,47] Additional treatments are needed, which increases the overall cost of the electrode fabrication. For instance, the addition of phosphoric acid[48] to control the pH of the slurry, the replacement of an aluminum foil with a carbon-coated Al current collector,[49] or the pre-treatment of an active material.[50] Recently,[51] efforts have been made to reduce the processing cost of lithium-ion batteries. According to a cost analysis,[51] 50% of the price of a lithium-ion battery comes from the composite electrode materials and current collectors. In addition to corrosion issues,[52] the current collector, and particularly the aluminum foil, drastically decreases the energy density of the battery.

To avoid these various problems, we investigated a new route for making electrodes without a binder or current collector.[53,54] Freestanding film electrodes have already been reported in the literature and are generally fabricated following a well-known paper-making process appropriate to the production of large numbers of electrodes. Cellulose-based electrodes avoid the use of a metal current collector because the active material and carbon additive are trapped in the porosity created by natural polymer filaments, leading to a self-standing and porous 3D structure.[55,56] However, a high amount of cellulose (binder) is needed in this case, thereby lowering the energy density of the electrodes. Alternatively, electrically conductive fibers such as vapor grown carbon fibers or carbon nanotubes can be used as both a binder and carbon additive,[57] although their price limits a scale-up of the fabrication method. In addition, the surface roughness of these electrodes leads to a poor contact with the separator used (e.g. Celgard) in the battery, and an inferior electrochemical performance is generally obtained. Our strategy applies a low-cost graphene powder as the carbon source and a binder for the formulation of the electrodes. This material is often used to create flexible freestanding films of a few micrometers through a vacuum filtration process.[58] Inspired by the paper making process, we deposited thin cathode ($LiFePO_4$ + graphene) and anode ($Li_4Ti_5O_{12}$ + graphene) layers on a Celgard-type separator used in battery manufacturing.[53]

The electrochemical performance of $LiFePO_4$ and $Li_4Ti_5O_{12}$ electrodes fabricated following a doctor-blade (conventional) method were compared to those of an electrode prepared using a new process with a Celgard membrane as support for the composite electrode material. A superior electrochemical performance was obtained for self-standing electrodes, particularly at high C-rates owing to the absence of a binder. $LiFePO_4$ electrodes on Celgard showed electronic conductivities of ~10 times higher than that of a composite cathode film on an aluminum current collector. The specific capacity of the $LiFePO_4$/Celgard electrodes was more than 6-times higher than that of a $LiFePO_4$ electrode coated on an Al foil. Finally, the specific capacity of a $LiFePO_4/Li_4Ti_5O_{12}$ full cell made using the film electrodes deposited on a Celgard membrane exhibited stable specific capacities during cycling at various C-rates and delivered approximately 106 $mAh.g^{-1}_{electrode}$ at a rate of C/10.

Experimental Section

Electrochemical exfoliation of graphite foil

Graphene powder was obtained using electrochemical exfoliation of a graphite foil (Alfa Aesar, 7.5 cm × 2 cm × 0.05 cm) connected to a positive terminal of a DC power supply.[59] The negative electrode was a Pt mesh (4 cm^2). Both electrodes were immerged in an aqueous 0.1 M H_2SO_4 solution and separated by 4 cm. Electrochemical exfoliation was carried out by applying a DC voltage of 6 V between the two electrodes. After 1 h of electrolysis, the solution containing exfoliated graphene sheets was vacuum filtrated with a Büchner assembly and a polytetrafluoroethylene (PTFE) membrane filter with a 0.47 μm pore size. The resulting powder was then washed several times with nanopure water to remove residual acid prior to dispersal in dimethylformamide (DMF) through an ultrasonication process for 10 min. The dispersion was left standing for 24 h to precipitate some thick

graphitic flakes, and only the upper part of the dispersion was collected. The resulting material was heat treated in a tubular furnace for 1 h at 1000 °C under an Ar/5% hydrogen gas mixture and subsequently used for creating the electrode, as described below.

Electrode preparation

Electrode material coated on aluminum foil

$LiFePO_4$/C (LFP, 2–3 wt% carbon) and $Li_4Ti_5O_{12}$ (LTO) powders were provided by Hydro-Québec, Montréal, Canada. The conventional fabrication method (see Scheme 1b) consists of mixing the active material (LFP or LTO powder) with polyvinylidene fluoride (PVDF) and acetylene black at a weight ratio of 80:10:10 using N-methyl-2-pyrrolidone (NMP, Alfa Aesar, 99%) as a solvent. The resulting slurry was cast on aluminum foil (15 μm thick) with a thickness of 50 μm and dried at 80 °C under a vacuum for 24 h. These electrodes are denoted as LFP/Al and LTO/Al.

Electrode material coated on a separator

For the preparation of electrodes on a separator[53] (see Scheme 1a), 80 wt% of an active material (LFP or LTO powder) was dispersed in 50 mL of DMF (or water) followed by 20 wt% of FLG. Additional experiments were carried out using 85 wt% LFP and 15 wt% FLG. The dispersion was placed in an ultrasonic bath for 30 min, and thereafter the mixture was filtrated using a Büchner assembly with a Celgard-2320 separator (thickness of 20 μm) as a filter. After 30 min, the film formed on the separator was left for 1 h before storage in an oven at 60 °C under a vacuum. These electrodes are denoted herein as LFP/Celgard and LTO/Celgard. All electrodes were cut into circular disks (area of 1.767 cm^2) with a mass loading ranging from 0.9 to 3.6 $mg.cm^{-2}$ depending on the material (LFP or LTO) or thickness of the electrodes. Figure 1 shows an example of a thin and homogeneous LFP/Celgard electrode. Figure 1b shows that the electrode is highly flexible without any evidence of cracks in the film.

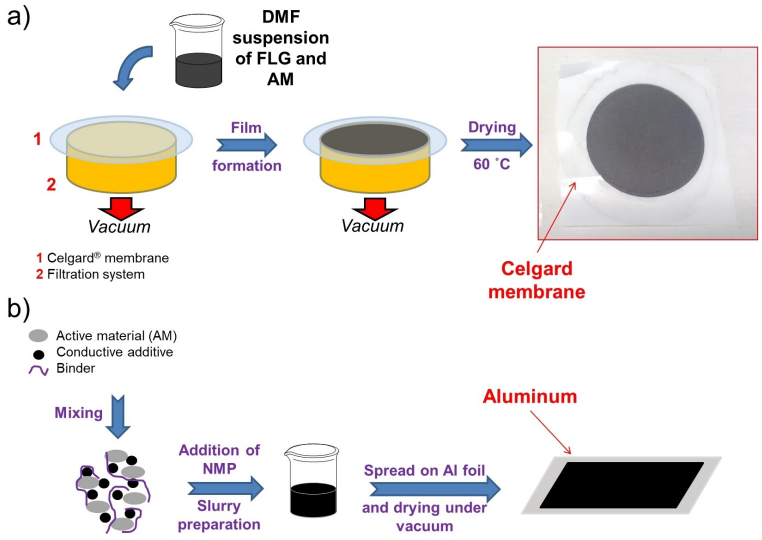

Scheme 1. Schematic illustration of the preparation of Li-ion electrodes: a) on a separator and b) using a conventional method. For preparation on a separator, a DMF mixture of few-layer graphene (FLG) and an active material (AM) is vacuum filtered until the formation of a homogeneous film occurs on the filter (Celgard membrane). After drying at 60 °C, the electrode is cut into a circular disk. For the conventional method (b), the active material is mixed with a conductive additive and a binder before obtaining a slurry by adding a small amount of NMP. After spreading the slurry on an aluminum foil and heating at 80 °C under a vacuum, the electrode is cut into a circular disk.

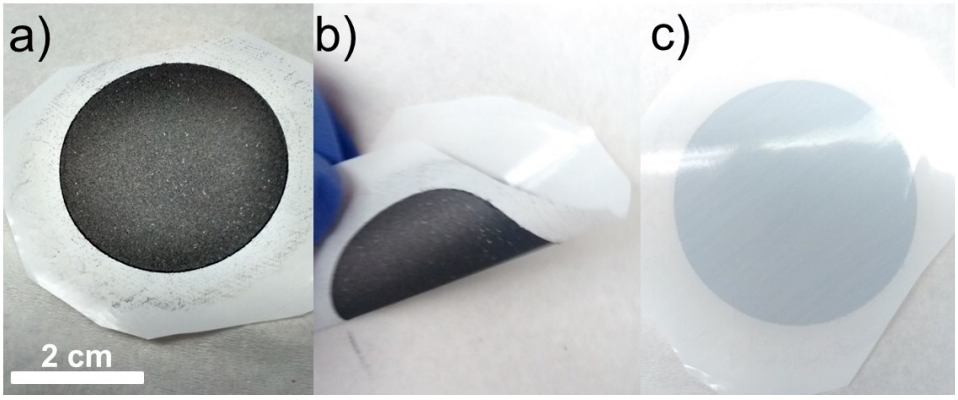

Figure 1. a) Top and c) bottom views of the LFP/Celgard electrode deposited on a Celgard-2320 separator. In (b), the film is flexible and remains intact under mechanical stress.

Electrochemical characterization

LFP/Al, LFP/Celgard, LTO/Al, and LTO/Celgard electrodes were characterized in two-electrode coin cells with lithium metal as a negative electrode, a Celgard®-2320 separator (except for LFP/Celgard or LTO/Celgard) in 1 M $LiPF_6$ in an ethylene carbonate (EC), diethyl carbonate (DEC), and dimethyl carbonate (DMC) (1:1:1 by volume) electrolyte. The cells were assembled in a dry argon-filled glove-box. The cells were controlled using a VMP3 potentiostat.

Charge/discharge cycling was applied in galvanostatic mode at between 2.0 to 4.0 V and 1.2 to 1.9 V versus Li/Li^+ for the LFP and LTO electrodes, respectively. Experiments were carried out after 1 h of rest at an open circuit voltage (OCV), and for each cycling rate ranging from C/10 to 10 C, ten cycles were recorded. In addition, a complete LFP/Celgard/electrolyte/LTO/Celgard cell with a LFP/LTO mass ratio of 1 (loading of electrodes of 0.9 $mg.cm^{-2}$) was also assembled by placing Celgard membranes face-to-face, as represented in Scheme 2. The cell was cycled between 1.0 to 2.5 V at various cycling rates ranging from C/10 to 5 C.

Electrochemical impedance spectroscopy (EIS) measurements were conducted with an amplitude of 10 mV and a frequency range of 200 kHz to 0.01 Hz. EIS data were collected after five cycles of charge/discharge at a C/2 rate and after 4 h of rest at OCV.

Characterization

Electronic conductivity measurements

Electronic conductivities of LFP/Celgard and LFP/Al cathode films were determined using a 4-point probe measurement using a Keithley 6220 DC precision current source (Signatone). To avoid the contribution of the aluminum current collector, inks used to prepare LFP/Al films were cast on glass slides. For LFP/Celgard electrodes, the resistance was directly measured for films formed on a separator. Current-voltage (DC voltage) sweeps were recorded at 100 $mV.s^{-1}$ and yielded a linear response. The electronic conductivity of the film electrode was calculated as follows [Eq. (1)]:

$$\sigma_e = \frac{1}{R \times e} \quad (1)$$

where σ_e is the electrical conductivity ($S.cm^{-1}$), R is the resistance of the film determined from the inverse slope of the current–voltage curve (Ω square), and e is the film thickness (cm).

Scanning electron microscopy measurement

The morphological studies of LFP electrode films were conducted using a scanning electron microscope JEOL JSM-7600F equipped with an EDS detector (Oxford Instruments, X-Max 80) at Ecole Polytechnique de Montréal's Center for Characterization and Microscopy of Materials (CM)[2].

2. Results and Discussion

2.1. Morphological Study of LFP Electrodes Using Scanning Electron Microscopy

Figure 2 shows SEM images of an LFP composite electrode on aluminum foil (a, b) and Celgard, before (c, d) and after (e, f) cycling. At low magnification (Figure 2c), the surface of an LFP/Celgard electrode is composed of small LFP particles ranging from several hundred nanometers to 1 μm, dispersed between and on graphene sheets. The method leads to thin electrodes with a good dispersion of materials (LFP and graphene). However, because calendering was not employed, the surface film does not appear completely flat, and some large graphene particles are randomly distributed. By contrast, the surface of the electrode made using a conventional method (see Figure 2a) is flatter but with several clusters of a few micrometers randomly dispersed. These clusters seem to be mainly composed of agglomerates of LFP in contact with the binder.

2.2. Electrochemical Behavior of LFP Electrodes

The electrochemical performances of LFP/Celgard and LFP/Al electrodes were evaluated in a half-cell using a Li anode. Typical charge/discharge profiles obtained for these electrodes are described in more detail below, where the electrochemical behavior of the full battery are discussed. Figure 3a shows the rate capability for LFP/Celgard half-cells for two mass loadings and for LFP/Al with intermediate loading. The discharge capacities were calculated by considering the total mass of the composite electrode except for LFP/Al, the capacities of which are reported by considering both the mass of the composite electrode and the aluminum current collector. At a low current

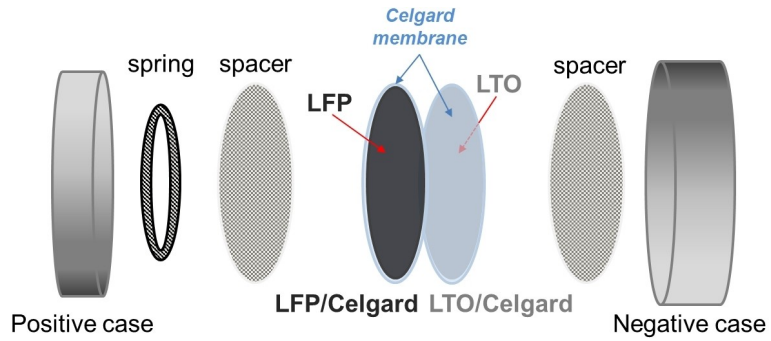

Scheme 2. Schematic illustration of coin-cell assemblage with LFP/Celgard and LTO/Celgard electrodes placed face-to-face (LFP/Celgard/Celgard/LTO) with no additional separator or current collectors. The electrolyte is not represented.

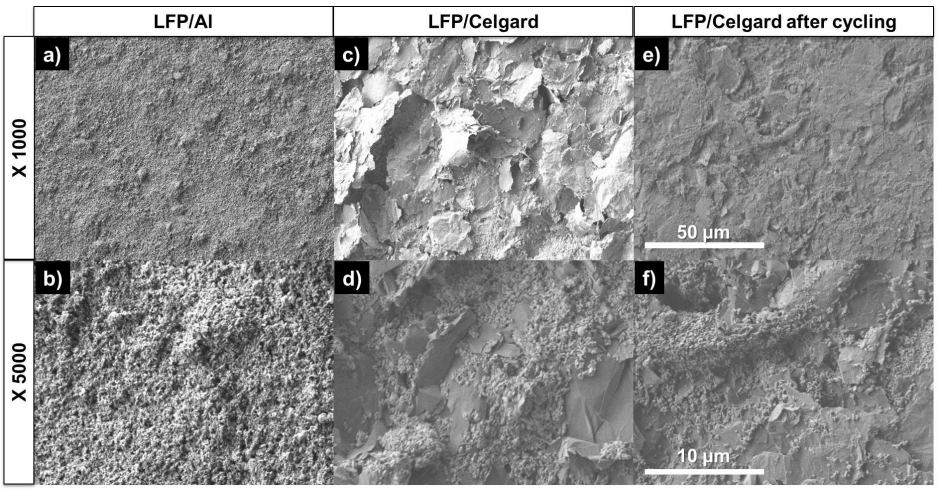

Figure 2. SEM images of LFP/Al electrode at magnifications of a) 1,000× and b) 5,000×, and LFP/Celgard electrodes; c), d) before; and e), f) after cycling. Images (c) and (e) were obtained at a magnification of 1,000× and images (d) and (f) were obtained at a magnification of 5,000×.

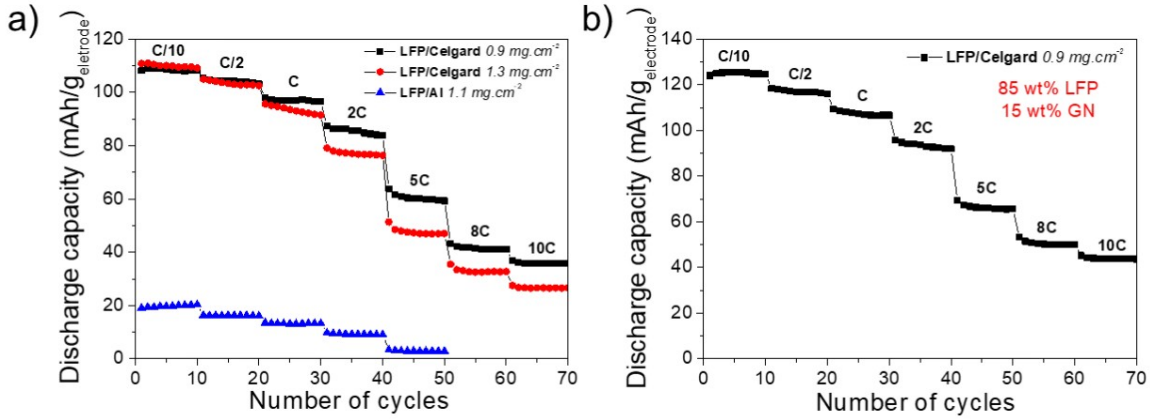

Figure 3. Rate capability of LFP/Celgard and LFP/Al half-cells (see Experimental Section for the electrode composition): a) the capacities reported with respect to the total mass of the composite electrodes except for LFP/Al, the capacities of which are also reported versus the mass of the composite electrode and the Al current collector, and the b) rate capability of the LFP/Celgard electrode with a higher loading of LFP (85 wt%) and 15 wt% of graphene. Please refer to the web version for the color codes used.

density (C/10), LFP/Celgard electrodes delivered discharge capacities of approximately 110 $mAh.g^{-1}_{electrode}$, which corresponds to more than 6-times the gravimetric capacity of LFP/Al (~20 $mAh.g^{-1}_{electrode}$). This result clearly highlights the importance of avoiding the use of a heavy current collector. As a representative example, the aluminum current collector of an LFP electrode with a loading of 3.6 $mg.cm^{-2}$ itself represents 47% of the electrode mass. This percentage dramatically increases for thinner electrodes. Similar results were recently reported for self-standing films made of carbon-coated $LiFePO_4$ and single-walled carbon nanotubes (SWNTs).[54] In the latter study, the Al current collector represented approximately 54 wt% of the LFP electrode, and at C/10, a specific capacity of ~120 $mAh.g^{-1}_{electrode}$ was reported for a self-standing electrode containing 80 wt% of the active material. For an LFP/Celgard electrode with the lowest loading (■), increasing the cycling rate to 2 C still allowed almost 80% of the initial capacity to be maintained at C/10. With the increase in the cycling currents, the discharge capacities gradually decreased; interestingly, however, at 10 C, approximately 1.5- and 2-times higher capacities per gram of electrode were obtained for the LFP/Celgard electrodes with a higher (●) and the lowest (■) loadings, respectively, in comparison to the LFP/Al electrode (▲). The superior capacity retention for the LFP/Celgard electrodes, even with the higher electrode mass loadings, was explained by the absence of a resistive binder and the use of a highly conductive graphene. In fact, electrochemically exfoliated graphene is known to exhibit a high electronic conductivity within the range of 10^1–10^2 $S.cm^{-1}$.[60,61] This was confirmed by measuring the resistance of LFP/Celgard and LFP/Al electrode films. Table 1 shows the electronic conductivity for the different films. Because 20 wt% graphene sheets were used in the composition of the electrode, the electronic conductivity values of LFP/Celgard electrodes were slightly smaller than

Table 1. Electronic conductivity of LFP/Celgard and LFP/Al electrodes.

Electrode	Loading [mg.cm^{-2}]	σ_e [S.cm^{-1}]
LFP/Celgard	0.9	2.31 ± 0.16
LFP/Celgard	1.3	2.28 ± 0.20
LFP/Al	1.1	0.24 ± 0.06

those reported for graphene films.[61] However, as expected, the electronic conductivities were one order of magnitude higher for the LFP/Celgard electrodes than for the LFP/Al film (see the Experimental section). The electronic conductivity of the LFP cathode spread on an aluminum current collector is similar to that reported in the literature.[54,62] More interestingly, the relative standard deviation of the electronic conductivity for two LFP/Celgard electrodes is much smaller (less than 9%) than that of the LFP/Al electrode (25%). This behavior is likely caused by non-uniform films owing to the presence of agglomerates (Figures 2a and 2b).

It is worth noting that graphene did not significantly contribute to the specific capacities of LFP/Celgard electrodes because less than 5 mAh.g^{-1} was obtained with a free-standing graphene electrode (see Figure SI1 in the Supplementary Information). Additional tests realized using only 15 wt% of graphene sheets to make a self-standing film revealed that the electrochemical performance (see Figure 3b) of LFP/Celgard electrodes composed of 20 wt% and 15 wt% of FLG were similar, even at a high C-rate. The electrode delivered approximately 125 mAh.g$^{-1}_{electrode}$ at C/10, which is comparable to the gravimetric capacity obtained for the LFP/SWNT composite containing 85 wt% of LFP.[54] This demonstrates that the graphene loading can be decreased to 15 wt%. Moreover, the mechanical resistance of the film was not significantly affected. However, with a lower amount of graphene (≤ 10 wt %), the mechanical resistance of the films was lower, and the electrochemical behavior of the resulting electrodes was not tested. Graphene is a 2D material displaying good mechanical properties owing to a π-stacking effect;[63] however, this physical effect is lost when its fraction in a composite film is too low. Alternatively, SWNTs can form a solid 3D network owing to an entanglement of nanofibers, and self-standing electrodes with 95 wt% of LFP can be obtained although under a low tensile stress (~2 ± 1 MPa).[54] In this latter case, however, the cost of such electrodes clearly prohibits a scale-up.

Electrochemical impedance spectroscopy measurements for LFP/Celgard (20 wt% of graphene sheets) and LFP/Al electrodes were also carried out. The Nyquist plots shown in Figure 4 indicate an intercept on the real axis at a high frequency, which is attributed to the resistance of the electrolyte, and as expected, these resistance values are extremely similar. A semicircle in the high-middle frequency region is observed for both electrodes, and the diameter on the Z_{re} axis is approximately equal to the charge transfer resistance through the electrode/electrolyte interface.[62] A charge transfer resistance of approximately 410 Ω was found for the LFP/Al electrode in comparison to only 150 Ω for the LFP/Celgard electrode. This drastic decrease in resistance is in accordance with the better cycling performance shown in Figure 3, and is attributed to the absence of a binder and to the good electrical contact between the LFP particles and highly conductive graphene sheets.

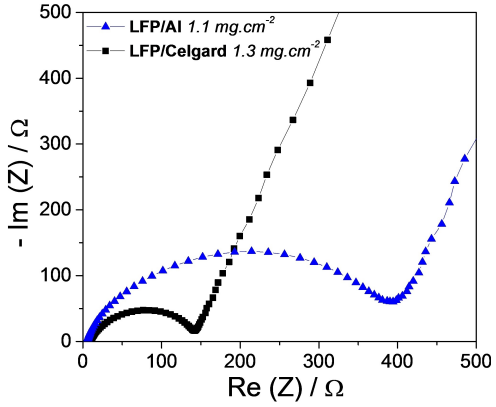

Figure 4. Electrochemical impedance spectroscopy measurements for LFP/Celgard and LFP/Al electrodes (see the Experimental Section for more details). Please refer to the web version for the color codes used.

The surface morphology of the LFP/Celgard electrode was also characterized after constant current cycling, a disassembly of the cell, and through the washing with DMC. Figure 2e shows that the film was smoother than before cycling (Figure 2c) because the pressure was applied to seal the coin cell. It is interesting to see that both FLG and LFP particles remain connected together (see Figure 2f) without a loss of film providing good evidence that the use of a binder can be avoided to fabricate electrodes of lithium-ion batteries.

2.3. Electrochemical Behavior of LTO Electrodes

LTO electrodes were prepared using conventional (LTO/Al) and new (LTO/Celgard) fabrication methods. The rate capability of these electrodes is shown in Figure 5. The loading of electrodes on Celgard was varied between 0.9 and 3.6 mg/cm^2. At a low C-rate, discharge capacities of between 95 and 105 mAh.g$^{-1}_{electrode}$ were obtained for LTO/Celgard electrodes. Interestingly, increasing the loading of the LTO/Celgard electrode by a factor of 4 did not adversely affect its electrochemical performance even at a high C-rate, presumably owing to the good dispersion of LTO between the graphene sheets. These results demonstrate that the new fabrication method can provide electrodes with high loading without affecting the performance. However, for both electrodes, an important capacity fading was observed when cycled at a rate of C/2. This is due to a low electronic conductivity of uncoated LTO material.[64] In particular, an LTO/Al electrode cannot efficiently cycle at 5 C, whereas an electrode made directly on Celgard delivered a rate of between 20 to 30 mAh.g$^{-1}_{electrode}$. Finally, at C/10, even with a loading of 4-times lower, the LTO/Celgard electrode (■) provided a specific capacity of 2.5-times larger than that of the LTO/Al electrode (★).

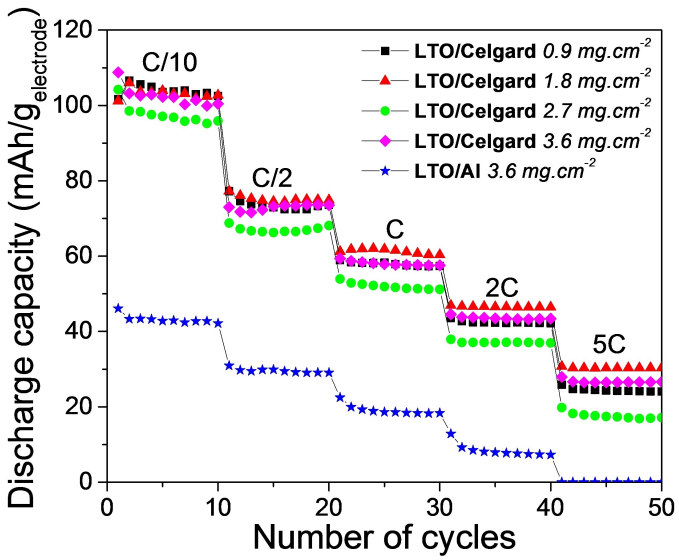

Figure 5. Rate capability of LTO/Celgard and LTO/Al electrodes with various mass loadings. Capacities are reported with respect to the total mass of the composite electrode except for LTO/Al, the capacities of which consider the mass of the composite electrode and aluminum current collector. Please refer to the web version for the color codes used.

2.4. Electrochemical Behavior of LFP/Celgard/Electrolyte/LTO/Celgard Full Cell

LFP/Celgard and LTO/Celgard electrodes were combined to make a complete Li-ion battery. The LTO anode was in a delithiated state, and 3 Li can theoretically be inserted. The reaction for the full cell is given by Eq. (2).

$$3\ LiFePO_4 + Li_4Ti_5O_{12} \rightarrow 3\ FePO_4 + Li_7Ti_5O_{12} \quad (2)$$

Because the theoretical capacity (175 mAh.g^{-1}) of LTO[65] is slightly higher but similar to that of LFP (170 mAh.g^{-1}), a LFP/LTO mass ratio close to 1 should be used for the cell assembly. This ratio was kept by taking into account the practical discharge capacities obtained above (i.e., 110 mAh.g$^{-1}_{electrode}$ for LFP and ~105 mAh.g$^{-1}_{electrode}$ for LTO). Figure 6a shows the charge/discharge profiles for the LFP/Celgard and LTO/Celgard electrodes in a half-cell (cycled versus Li metal) at a rate of C/10. The practical capacity for both electrodes is lower than the theoretical capacity (132 mAh.g$^{-1}_{electrode}$ for LFP and 140 mAh.g$^{-1}_{electrode}$ for LTO) because of the different limitations in the Li-ion cells and particularly in research-type cells such as coin or pouch cells.[66] LFP and LTO electrodes show a flat plateau owing to the two-phase reaction occurring at 3.4 and 1.55 V versus Li/Li$^+$, respectively.[67] Figure 6b shows a typical charge/discharge plateau of 1.9 V for the complete LFP/Celgard/electrolyte/LTO/Celgard full cell assembled with electrodes whose charge/discharge profiles are as shown in Figure 6a.[68] The discharge capacity of 106 mAh.g$^{-1}_{electrode}$ is similar of that of the LTO/Celgard electrode, which limits the capacity of the full cell in this case.

The rate capability of the LFP/Celgard/electrolyte/LTO/Celgard full cell is shown in Figure 7. The discharge capacities for each applied current was within the same range as those obtained for the LTO/Celgard electrodes shown in Figure 5. For instance, at 5 C, the average discharge capacity for the LFP/Celgard electrode (see Figure 3) was approximately 60 mAh.g^{-1}, whereas only 25–30 mAh.g^{-1} was obtained for both LTO/Celgard (Figure 5) and LFP/Celgard/electrolyte/LTO/Celgard batteries (Figure 7). Despite its interesting aspects, the LTO anode described in the present study clearly limits the electrochemical performance. Nonetheless, we demonstrated that the method involving the deposition of an active material on a separator has proven to be efficient at creating battery electrodes without the use of an aluminum current collector and binder. Nevertheless, these preliminary studies must be complemented by an optimization of the experiment conditions and the use of better benchmark materials.

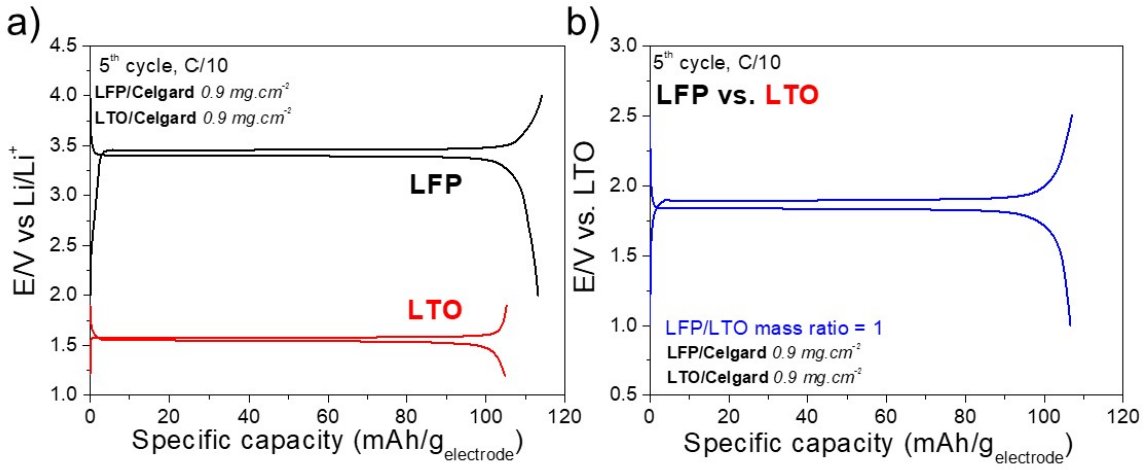

Figure 6. Charge/discharge profiles for the fifth cycle at a C-rate of C/10 for a) $LiFePO_4$/C (LFP, black line) and $Li_4Ti_5O_{12}$ (LTO, red line) electrodes cycled versus Li metal, and b) a full battery LFP vs. LTO with an LFP/LTO mass ratio of 1. All electrodes were made on Celgard without an aluminum current collector.

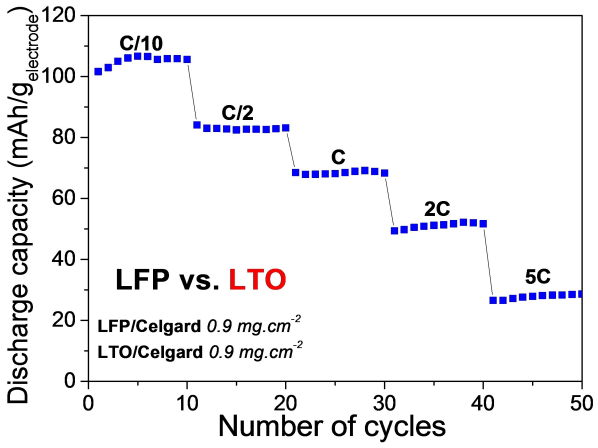

Figure 7. Rate capability of a full LFP/LTO battery with balanced electrodes. The electrodes were made according to the new fabrication method. The specific capacities are reported with respect to the total mass of the cathode composite.

2.5. Advantages of the New Fabrication Method

An electrode fabrication process involving the deposition of composite electrode materials on a separator and not requiring either a binder or a current collector was developed. This can potentially decrease the fabrication cost of a battery to a considerable extent. A toxic and costly NMP is replaced with a cheaper and much lower boiling temperature solvent such as DMF, enabling a lower temperature drying step, and using water for a greener process. Moreover, the process is rapid, simple, and can be developed using the current industrial paper-making infrastructure. More specific to the laboratory scale process described in this manuscript, a continuous vacuum permits rapidly drying the film formed on a Celgard separator, before drying at only 60 °C. Moreover, the time needed for electrode preparation is significantly shortened. The grinding, mixing of components (a conductive additive, a binder, and an anode/cathode material), and preparation of a slurry are replaced with a single step involving the mixing of an active electrode material and graphene, leading to a thin and homogeneous film applied directly on the separator. Thus, the cells can be assembled by placing an LFP/Celgard bilayer in contact with a lithium foil (half-cell) or with an LTO/Celgard bilayer with Celgard layers contacting each other (a full cell, as shown in Scheme 2). In addition, because a current collector is not employed, the energy density of the Celgard-based electrode is also increased.

3. Conclusions

The new method for fabricating lithium-ion electrodes described herein, which applies a Celgard membrane as an active electrode material support, does not require a heavy aluminum foil current collector, a binder and a toxic solvent. It was also demonstrated that graphene sheets can be used as an additive in the manufacturing of such Celgard-based electrodes. Moreover, using a single step, an electrode film was formed on the separator used in a battery. A Celgard-based electrode is flexible, shows a good mechanical resistance, and permits assembling a cathode with an anode, both of which can be fabricated using this technique, to make a flexible lithium-ion battery. The electrochemical behavior of the LFP and LTO electrodes fabricated following this process showed superior electrochemical performance compared to those prepared by a conventional method owing to the absence of a binder and the use of conductive graphene. $LiFePO_4$ electrodes delivering up to 125 $mAh.g^{-1}_{electrode}$ were obtained, which corresponds to more than 6-times the gravimetric capacity of an LFP/Al electrode (~20 $mAh.g^{-1}_{electrode}$), when both the electrode material and the current collector are taken into account. Moreover, an LFP/LTO flexible full cell was assembled and showed excellent stability during the cycling with a capacity of 106 $mAh.g^{-1}_{electrode}$ at C/10.

Although the feasibility of the approach has been demonstrated, further characterization of the composition of the active material and Celgard structure is required to determine the distribution of active materials within the thickness of the Celgard-based electrode. Issue such as a potential short circuit between the electrodes of the cell must be avoided, particularly if the anode and cathode electrode materials are deposited on opposite sides of a single Celgard membrane. Future studies will focus on the optimization of the electrochemical performance, using different graphene materials and changing the LFP and LTO particle sizes and shapes. For instance, the use of hollow melon-seed-shaped $LiFePO_4$ microplates with large {010} surfaces will be strongly appropriate for use with the new fabrication method.[69] Additionally, increasing the active material loading and optimizing the active material/graphene sheets ratio will be the aim of future studies to clearly demonstrate the utility of this fabrication method. In parallel, better benchmark materials will be utilized.

Acknowledgements

This work was financially supported by Hydro-Québec and NSERC (CRD and Discovery grants). This research also benefited from the use of the research infrastructure of NanoQAM (http://www.nanoqam.uqam.ca/services.php?lang=en), which is also acknowledged.

Conflict of Interest

The authors declare no conflict of interest.

Keywords: Celgard separator · high-energy density · self-standing electrode · graphene · collector-free electrode; binder-free electrode

[1] J. Li, Z. Du, R. E. Ruther, S. J. An, L. A. David, K. Hays, M. Wood, N. D. Phillip, Y. Sheng, C. Mao, S. Kalnaus, C. Daniel, D. L. Wood III, *JOM* **2017**, *69*, 1484–1496.
[2] T. Mayer, D. Kreyenberg, J. Wind, F. Braun, *Int. J. Hydrogen Energy.* **2012**, *37*, 14463–14474.
[3] K. S. Nanjundaswamy, H. D. Friend, C. O. Kelly, D. J. Standlee and R. L. Higgins, "Electrode fabrication for Li-ion: processing, formulations and defects during coating," IECEC-97 Proceedings of the Thirty-Second Intersociety Energy Conversion Engineering Conference (Cat. No.97CH6203), Honolulu, HI, USA, **1997**, *1*, 42–45.
[4] S. M. Spearing, *Acta Mater.* **2000**, *48*, 179–196.
[5] D. A. Lavan, T. Mcguire, R. Langer, *Nat. Biotechnol.* **2003**, *21*, 1184–1191.
[6] J. D. Fowler, M. J. Allen, V. C. Tung, Y. Yang, R. B. Kaner, B. H. Weiller, *ACS Nano* **2009**, *3*, 301–306.
[7] K. Sun, T.-S. Wei, B. Y. Ahn, J. Y. Seo, S. J. Dillon, J. A. Lewis, *Adv. Mater.* **2013**, *25*, 4539–4543.
[8] K. Fu, Y. Wang, C. Yan, Y. Yao, Y. Chen, J. Dai, S. Lacey, Y. Wang, J. Wan, T. Li, Z. Wang, Yue Xu, L. Hu, *Adv. Mater.* **2016**, *28*, 2587–2594.
[9] J. W. Long, B. Dunn, D. R. Rolison, H. S. White, *Chem. Rev.* **2004**, *104*, 4463–4492.
[10] M. Gabard, M. Zaghrioui, D. Chouteau, V. Grimal, T. Tillocher, F. Ghamouss, N. Poirot, *Chem. Eng.* **2017**, *1*, 5.
[11] X. Zhou, A.-M. Cao, L.-J. Wan, Y.-G. Guo, *Nano Res.* **2012**, *5*, 845–853.
[12] Y. Zhang, Y. Li, X. Xia, X. Wang, C. Gu, J. Tu, *Sci. China Technol. Sc.* **2015**, *58*, 1809–1828.
[13] M. E. Spahr, Carbon-Conductive Additives for Lithium-Ion Batteries, In: M. Yoshio, R. J. Brodd, A. Kozawa, Lithium-Ion Batteries. *Springer*, **2009**, New York, NY.
[14] X.-M. Liu, Z. D. Huang, S. W. Oh, B. Zhang, P.-C. Ma, M. M. F. Yuen, J.-K. Kim, *Compos. Sci. Technol.* **2012**, *72*, 121–144.
[15] N. Delaporte, R. L. Belanger, G. Lajoie, M. Trudeau, K. Zaghib, *Electrochim. Acta* **2019**, *308*, 99–114.
[16] A. Gambou-Bosca, D. Bélanger, *J. Electrochem. Soc.* **2015**, *162*, A5115-A5123.
[17] S. Deville, *Adv. Energy Mater.* **2008**, *10*, 155–169.
[18] J. H. Um, M. Choi, H. Park, Y.-H. Cho, D. C. Dunand, H. Choe, Y.-E. Sung, *Sci. Rep.* **2016**, *6*, 18626.
[19] T. Yuan, B. Zhao, R. Cai, Y. Zhou, Z. Shao, *J. Mater. Chem.* **2011**, *21*, 15041–15048.
[20] C. H. Chen, E. M. Kelder, M. J. G. Jak, J. Schoonman, *Solid State Ionics* **1996**, *86–88*, 1301–1306.
[21] W.-S. Yoon, S.-H. Ban, K.-K. Lee, K.-B. Kim, M. G. Kim, J. M. Lee, *J. Power Sources* **2001**, *97–98*, 282–286.
[22] M. Al-Shroofy, Q. Zhang, J. Xu, T. Chen, A. P. Kaur, Y.-T. Cheng, *J. Power Sources* **2017**, *352*, 187–193.
[23] S. Shiraki, H. Oki, Y. Takagi, T. Suzuki, A. Kumatani, R. Shimizu, M. Haruta, T. Ohsawa, Y. Sato, Y. Ikuhara, T. Hitosugi, *J. Power Sources* **2014**, *267*, 881–887.
[24] L. Baggeto, R. R. Unocic, N. J. Dudney, G. M. Veith, *J. Power Sources* **2012**, *211*, 108–118.
[25] B. Ludwig, Z. Zheng, W. Shou, Y. Wang, H. Pan, *Sci. Rep.* **2016**, *6*, 23150.
[26] S. Koike, K. Tatsumi, *J. Power Sources* **2007**, *174*, 976–980.
[27] A. Gören, J. Mendes, H. M. Rodrigues, R. E. Sousa, J. Oliveira, L. Hilliou, C. M. Costa, M. M. Silva, S. Lanceros-Méndez, *J. Power Sources* **2016**, *334*, 65–77.
[28] H. W. Choi, T. Zhou, M. Singh, G. E. Jabbour, *Nanoscale* **2015**, *7*, 3338–3355.
[29] W. Bauer, D. Nötzel, *Ceram. Int.* **2014**, *40*, 4591–4598.
[30] H. Dreger, H. Bockholt, W. Haselrieder, A. Kwade, *J. Electron. Mater.* **2015**, *44*, 4434–4443.
[31] D. J. Kirsch, S. D. Lacey, Y. Kuang, G. Pastel, H. Xie, J. W. Connell, Y. Lin, L. Hu, *ACS Appl. Energy Mater.* **2019**, *2*, 2990–2997.
[32] W. Blake Hawley, J. Li, *J. Energy Storage* **2019**, *25*, 100862.
[33] G.-W. Lee, J. H. Ryu, W. Han, K. H. Ahn, S. M. Oh, *J. Power Sources* **2010**, *195*, 6049–6054.
[34] D. L. Wood, J. D. Quass, J. Li, S. Ahmed, D. Ventola, C. Daniel, *Drying Technol.* **2018**, *36*, 234–244.
[35] K. Miyata, T. Kawada, K. Katou. NMP distilling apparatus. European Patent Application No. 10815325.5.
[36] M. Baunach, S. Jaiser, S. Schmelzle, H. Nirschl, P. Scharfer, W. Schabel, *Drying Technol.* **2016**, *34*, 462–473.
[37] D. Popovici, M. Meunier, E. Sacher, *J. Adhes.* **1999**, *70*, 155–166.
[38] M. Wentker, M. Greenwood, J. Leker, *Energies* **2019**, *12*, 504.
[39] A. Guerfi, M. Kaneko, M. Petitclerc, M. Mori, K. Zaghib, *J. Power Sources* **2007**, *163*, 1047–1052.
[40] J. Li, R. B. Lewis, J. R. Dahn, *Electrochem. Solid-State Lett.* **2007**, *10*, A17-A20.
[41] F. A. Çetinel, W. Bauer, *Bull. Mater. Sci.* **2014**, *37*, 1685–1690.
[42] Z. Du, K. M. Rollag, J. Li, S. J. An, M. Wood, Y. Sheng, P. P. Mukherjee, C. Daniel, D. L. Wood III, *J. Power Sources* **2017**, *354*, 200–206.
[43] M. Kuenzel, D. Bresser, T. Diemant, D. V. Carvalho, G.-T. Kim, R. J. Behm, S. Passerini, *ChemSusChem* **2018**, *11*, 562–573.
[44] J. Li, C. Daniel, S. J. An, D. Wood, *MRS advances* **2016**, *1*, 1029–1035.
[45] D. Aurbach, B. Markovsky, G. Salitra, E. Markevich, Y. Talyossef, M. Koltypin, L. Nazar, B. Ellis, D. Kovacheva, *J. Power Sources* **2007**, *165*, 491–499.
[46] J.-F. Martin, M. Cuisinier, N. Dupré, A. Yamada, R. Kanno, D. Guyomard, *J. Power Sources* **2011**, *196*, 2155–2163.
[47] M. Bichon, D. Sotta, N. Dupré, E. De Vito, A. Boulineau, W. Porcher, B. Lestriez, *ACS Appl. Mater. Interfaces* **2019**, *11*, 18331–18341.
[48] W. Bauer, F. Cetinel, M. Muller, U. Kaufmann, *Electrochim. Acta* **2019**, *317*, 112–119.
[49] T. Tanabe, T. Gunji, Y. Honma, K. Miyamoto, T. Tsuda, Y. Mochizuki, S. Kaneko, S. Ugawa, H. Lee, T. Ohsaka, F. Matsumoto, *Electrochim. Acta* **2017**, *224*, 429–438.
[50] Process for Protecting Electrode Materials Against Moisture, Patent No. WO/2016/187699.
[51] D. L. Wood III, J. Li, C. Daniel, *J. Power Sources* **2015**, *275*, 234–242.
[52] T. Ma, G.-L. Xu, Y. Li, L. Wang, X. He, J. Zheng, J. Liu, M. H. Engelhard, P. Zapol, L. A. Curtiss, J. Jorne, K. Amine, Z. Chen, *J. Phys. Chem. Lett.* **2017**, *8*, 1072–1077.
[53] Flexible Electrode-Separator Elements And Processes For Their Preparation, Patent No. WO2018/014137 A1.
[54] T. Bibienne, L. Maillaud, S. Rousselot, L. W. Taylor, M. Pasquali, M. Dollé, *J. Solid State Electrochem.* **2017**, *21*, 1407–1416.
[55] L. Jabbour, C. Gerbaldi, D. Chaussy, E. Zeno, S. Bodoardo, D. Beneventi, *J. Mater. Chem.* **2010**, *20*, 7344–7347.
[56] N. Delaporte, G. Lajoie, S. Colin-Martin, K. Zaghib, *Sci. Rep.* **2020**, *10*, 3812.
[57] C. Ban, Z. Wu, D. T. Gillaspie, L. Chen, Y. Yan, J. L. Blackburn, A. C. Dillon, *Adv. Mater.* **2010**, *22*, E145-E149.
[58] R. Wang, C. Xu, J. Sun, L. Gao, C. Lin, *J. Mater. Chem. A* **2013**, *1*, 1794–1800.
[59] Methods of Forming Graphene by Graphite Exfoliation, Patent No. CA2803772 A1.
[60] C.-Y. Su, A.-Y. Lu, Y. Xu, F.-R. Chen, A. N. Khlobystov, L.-J. Li, *ACS Nano* **2011**, *5*, 2332–2339.
[61] B. D. Ossonon, D. Bélanger, *Carbon* **2017**, *111*, 83–93.
[62] N. Delaporte, A. Perea, E. Lebègue, S. Ladouceur, K. Zaghib, D. Bélanger, *ACS Appl. Mater. Interfaces* **2015**, *7*, 18519–18529.
[63] G. A. Ferrero, M. Sevilla, A. B. Fuertes, *Sustain. Energ. Fuels* **2017**, *1*, 127–137.
[64] T. Doi, Y. Iriyama, T. Abe, Z. Ogumi, *Chem. Mater.* **2005**, *17*, 1580–1582.
[65] K. Zaghib, M. Simoneau, M. Armand, M. Gauthier, *J. Power Sources* **1999**, *81–82*, 300–305.
[66] B. R. Long, S. G. Rinaldo, K. G. Gallagher, D. W. Dees, S. E. Trask, B. J. Polzin, A. N. Jansen, D. P. Abraham, I. Bloom, J. Bareño, J. R. Croy, *J. Electrochem. Soc.* **2016**, *163*, A2999-A3009.
[67] K. M. Colbow, J. R. Dahn, R. R. Haering, *J. Power Sources* **1989**, *26*, 397–402.
[68] K. Zaghib, M. Dontigny, P. Perret, A. Guerfi, M. Ramanathan, J. Prakash, A. Mauger, C. M. Julien, *J. Power Sources* **2014**, *248*, 1050–1057.
[69] X.-F. Yang, J.-H. Yang, Y. L. Zhong, V. Gariepy, M. L. Trudeau, K. Zaghib, J. Y. Ying, *ChemSusChem* **2014**, *7*, 1618–1622.

Manuscript received: December 27, 2019
Revised manuscript received: March 6, 2020
Version of record online: March 26, 2020